Error analysis of the pu in-situ absorption measurements in terms of background noise

Fanyu Meng, Tales Marini Storani, Daniel Fernandez Comesana

ERROR ANALYSIS OF THE PU IN-SITU SOUND ABSORPTION MEASUREMENTS IN TERMS OF BACKGROUND NOISE

Fanyu Meng **Tales Storani** **Dani Fernandez**

Microflown Technologies, Tivolilaan 205, 6824 BV Arnhem, the Netherlands

meng@microflown.com

ABSTRACT

Several measurement techniques are available for the determination of the acoustic properties of materials. Kundt's tube and reverberation room methods are widely used as standardized methods in laboratory environments, and thus not applicable in-situ. However, the acoustic properties can be changed when the materials are deformed or moved away from the original mounting for laboratory measurements. Several in-situ methods have been proposed, among which the PU in-situ method outperforms in terms of strong restriction of background noise and reflections, and a broad frequency range (typically from 300 Hz up to 10 kHz). This in-situ technique relies on direct measurements of sound pressure and acoustic particle velocity using a sound intensity PU probe. Acoustic impedance, sound reflection and acoustic absorption coefficients can be estimated by combining the measured data with an acoustic model. There are multiple sources of uncertainties that can bias the in-situ estimation, such as the measurement environment, measurement setup, material of the tested sample and calculation model. This paper focuses on the background noise as the uncertainty source and elaborates the background noise with added white noise and an external source of white noise to fully understand the influence of signal-to-noise ratio (SNR) to the calculation accuracy of the absorption coefficient.

1. INTRODUCTION

Acoustic absorbing materials are widely used in many different applications in order to offer a better environment or in a product composition. These samples are important in reducing sound energy from unwanted noise sources and lowering noise pollution as could be seen at [1]. The characterization of acoustic material properties has been the subject of extensive research as they are an essential input to acoustic simulations [2, 3].

Understanding its acoustic properties leads to a effective and aimed usage as well a better acoustic controlled and predictable situation. Non-acoustic specific and intrinsic properties, such as flow resistivity, tortuosity, density or porosity are often used in combination with empirical models and theoretical equations to determine acoustic properties of materials: impedance, absorption and reflection.

The surface impedance and absorption coefficient can be determined based on standardized methods, such as the Kundt's tube method [4] and the reverberation room method [5]. However, the standardized methods require laboratory environments, which are not always available. In addition, the samples under test have to be treated to fulfil the requirements. The acoustic properties of materials can then be changed, for example, through deformation or being moved away from the original mounting.

The limitations using the standardized laboratory measurement methods mentioned above suggest the necessity of introducing in-situ methods to characterize the acoustic properties of materials. Most of current in-situ methods are microphone-based, being single or multiple [6]. Alternatively, a PU in-situ method was proposed to calculate the surface impedance and then the absorption coefficient [1]. A PU probe contains one microphone, and one Microflown that measures particle velocity directly. The "figure of 8" directivity of the Microflown sensor enables a strong restriction of background noise [7]. Apart from this, the particle velocity can be measured directly in a broad frequency range, without frequency constraint if derived by pressure gradient. The PU method has been widely used for in-situ material measurements, such as the interior materials of vehicles [8], road surfaces [9] and theatres [10].

Due to uncontrolled conditions, the accuracy of in-situ PU measurements can usually be deteriorated by the measurement environments, measurement setup or the material of the test sample. Besides, different calculation models also lead to calculation variations in impedance and absorption coefficient [11, 12]. The material geometry and reflections from other objects were investigated based on BEM simulations in [6]. Deviations of the absorption coefficient can be observed when material surface is curved or in the presence of surrounding objects. Measurement setup was examined and it was found that the setup uncertainty affects more low absorbent samples [13]. The relationship between sample size and sensor probe height was intensively studied and some recommendations were given in [14].

Background noise, as an important factor that introduces measurement uncertainties in the PU in-situ method, has been limitedly investigated to the best of the authors knowledge. External loudspeakers were applied, and certain conclusions on the signal-to-noise ratio (SNR) of the external sound source and source angle are provided in

[1, 15]. However, the conclusions were merely based on limited amount of measurements, and detailed reasons on the signal level were missing. Other types of noise should also be considererd, for instance, self noise in the sensors. This paper elaborates the background noise with two different types, added white noise and external source to fully understand how they influence the signals and the calculated absorption coefficient. Frequency dependent SNRs of the sound pressure and particle velocity are inspected. In addition to the type of the noise, the receiver height, material type and the angle of the external source are also taken into account to study the error of the absorption coefficient. The SNR of background noise can be an indicator to check the quality of the PU in-situ measurements to assure an accurate calculation of the absorption coefficient.

2. SOUND FIELD MODEL ABOVE A SAMPLE OF MATERIAL

The absorption coefficient of a material surface is defined as, if no sound transmission is considered,

$$\alpha = \frac{I_i - I_r}{I_i} = 1 - |R|^2 \tag{1}$$

where I_i and I_r are the incident and reflected sound intensity, and R is the reflection factor [16]. This equation demonstrates that the absorption coefficient can be derived either by intensity or by reflection factor, the latter of which can be calculated by impedance. This work focuses on the reflection/impedance based approach.

The reflection factor R is calculated by the surface impedance Z_s. There are three ways to do so: plane wave, mirror source and Q-term models [1, 11]. The Q-term model takes spherical reflection into consideration and has been proved to be more accurate than the other two models [11, 13]. Thus this model will be applied in the following contents.

The impedance at the receiver can be calculated by the sound pressure p and particle velocity u

$$Z_r = \frac{p}{u}, \tag{2}$$

where

$$p = \frac{e^{-\mathrm{j}k(h_s-h)}}{h_s-h} + Q\frac{e^{-\mathrm{j}k(h_s+h)}}{h_s+h} \tag{3}$$

and

$$u = \frac{1}{\rho c}\left(\frac{e^{-\mathrm{j}k(h_s-h)}}{h_s-h}\left(\frac{1}{\mathrm{j}k(h_s-h)}+1\right) - Q\frac{e^{-\mathrm{j}k(h_s+h)}}{h_s+h}\left(\frac{1}{\mathrm{j}k(h_s+h)}+1\right) + \frac{\partial Q}{\partial h}\frac{e^{-\mathrm{j}k(h_s+h)}}{\mathrm{j}k(h_s+h)}\right). \tag{4}$$

Here, ρ is the air density, c is the speed of sound, h_s is the source height, h is the receiver height, k is the wavenumber, and Q is the spherical reflection factor which is denoted as

$$Q(Z_s, h, h_s) = 1 - \frac{2k}{Z_s}\frac{h_s+h}{e^{-\mathrm{j}k(h_s+h)}}\int_0^\infty e^{-q\frac{k}{Z_s}}\frac{e^{-\mathrm{j}k(h_s+h-\mathrm{j}q)}}{h_s+h-\mathrm{j}q}\mathrm{d}q. \tag{5}$$

Z_s cannot be directly solved from Equation. (2), and thus Secant Method was introduced to derive Z_s iteratively [11]. $Q(Zs, h, h_s)$ is subsequently calculated with known Z_s. Since obtaining the absorption coefficient α is the final goal of this work, Equation. (1) has to be adapted to for the Q-term model. It can be seen that Q depends on the surface impedance Z_s of the material, receiver height h and source height hs. Hence the reflection factor represents the reflection at the material surface when $h = 0$. The absorption coefficient is thus denoted by the spherical reflection factor

$$\alpha = 1 - |Q(Z_s, 0, hs)|^2. \tag{6}$$

3. SIMULATION OF MEASUREMENT ENVIRONMENTS

The PU probe based impedance measurement is simulated. The sound pressure and particle velocity fields above an infinite locally reactive plane are simulated by Equation. (3) and Equation. (4), where spherical reflections are assumed. The surface impedance is predicted by the Delany and Bazley model [17].

Two ways of simulating extraneous noise in in-situ measurement environments are investigated: directly added white noise (AWN) to the pressure and velocity signals at the receiver, and an external source of white noise (ESWN). The source and receiver are vertically aligned, with a distance of 0.26 m, which remains constant in the simulations. The source-receiver distance follows the source-probe distance of the in-situ absorption system of Microflown [1].

In the AWN case, the signal-to-noise ratio (SNR), receiver height h and frequency dependent SNR of the sound pressure P_{SNR} and particle velocity U_{SNR} are taken as variables to evaluate the absolute error of absorption coefficient $E(\alpha)$. For the ESWN case, the external source is placed 10 m away from the receiver. Along with the previously mentioned variables, the angle θ of the external source is studied. In the simulations, P_{SNR} is taken as reference. The simulation setup is shown in Figure. 1. An absorbent material (absorber) and a reflective material (reflector) are simulated with a flow resistivity σ of $2 \times 10^4\,\mathrm{kg\,m^{-3}\,s^{-1}}$ and $5 \times 10^6\,\mathrm{kg\,m^{-3}\,s^{-1}}$, respec-

tively. The flow resistivity is integrated in the Delany and Bazley model to calculate the surface impedance.

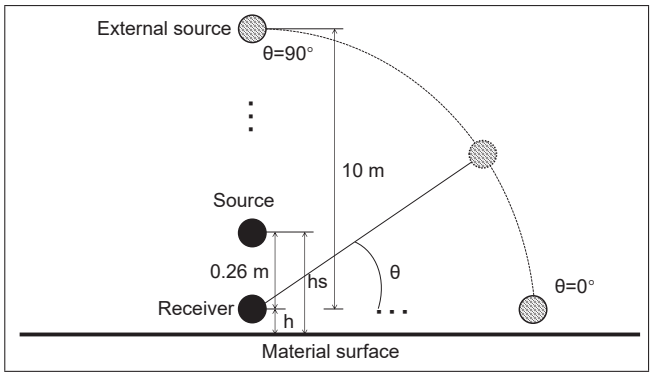

Figure 1. Simulation setup.

4. ANALYSIS OF EXTRANEOUS NOISE

4.1 Added white noise (AWN)

The receiver height h is set to 0.005 m, 0.015 m and 0.03 m, and P_{SNR} is changed from 10 dB to 40 dB with 10 dB interval. With $h = 0.015$ m, the calculated absorption coefficient, sound pressure and particle velocity of different SNRs and the two materials are shown in Figure. 2. The absorption coefficient is smoothed by moving median, and the pressure and velocity are smoothed by moving average. It is not surprising that the deviation in the absorption coefficient increases as the SNR decreases, except that at high frequencies the SNR has limited significance on deviating the absorption coefficient of the absorber. For both materials, the SNR of the particle velocity is relatively low at low frequencies.

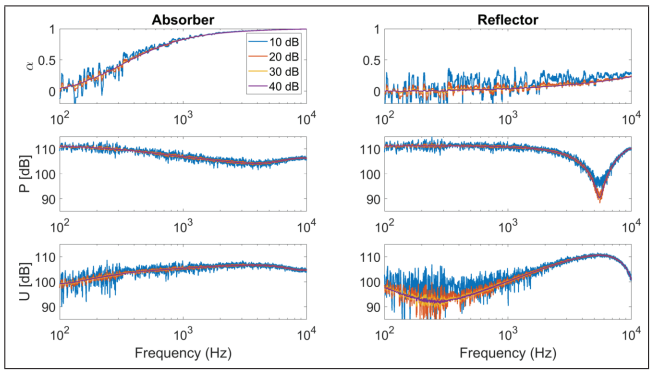

Figure 2. Absorption coefficient, and sound pressure and particle velocity at the receiver with $h = 0.015$ m.

Figure. 3 and Figure. 4 present the absolute errors of the absorption coefficient $E(\alpha)$, as well as the frequency dependent SNR of the pressure (P_{SNR}) and particle velocity (U_{SNR}). The equal SNR contours confirm that the both P_{SNR} and U_{SNR} are frequency dependent, which indicates that the overall SNR would not be sufficient to explain the variable behavior of the absorption deviation in a broadband frequency range. For the absorber in Figure. 3, the low U_{SNR} at low frequencies is more significant on causing the large deviation of absorption coefficient than P_{SNR}, because P_{SNR} varies little as the frequency changes. Whereas for the reflector in Figure. 4, although U_{SNR} could reach -15 dB with the overall SNR of the particle velocity being 10 dB, $E(\alpha)$ does not show its frequency dependency as what is shown for the absorber.

According to the results in [11], when the frequency is above 1 kHz, the three impedance models deliver quite similar surface impedance. The results at high frequencies calculated by a simpler model are reliable as well. The plane wave impedance model is denoted as

$$\alpha = 1 - |R|^2 = 1 - |\frac{Z_r - 1}{Z_r + 1}|^2, \tag{7}$$

where $Z_r = p/u$ as in Equation. (2). At high frequencies, the energy is mostly absorbed and barely reflected back to the receiver, therefore p and u are much the measures of the incident wave, which is the case for the absorber at high frequencies. In addition, the receiver is in the far field. These factors result in p and u are of similar amplitude and phase. However, for the reflector, different standing wave patterns due to reflections lead to large amplitude difference between p and u and phase mismatch at high frequencies. Therefore, large deviations still exist at high frequencies for the reflector.

Note that negative absorption coefficient is observed at low frequencies for both materials with the presence of noise, under the condition that the absorption coefficient is low. The conclusion can be drawn here that the low U_{SNR} is the main reason for the negative values compared to P_{SNR}. Another observation is that as the receiver height increases, the error of absorption coefficient slightly decreases in the low frequencies. This can also be explained by the increment of U_{SNR} as the height increases, despite P_{SNR} decreases.

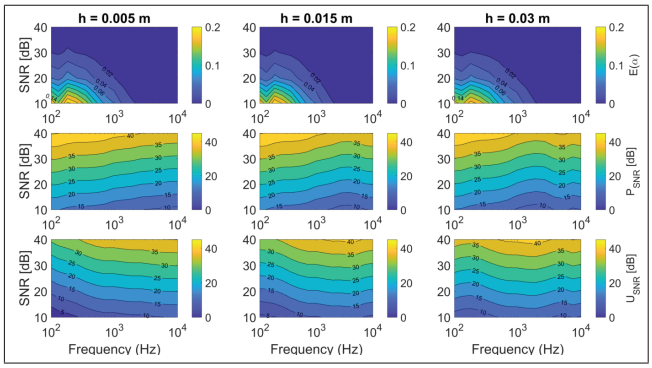

Figure 3. Absolute error of absorption coefficient $E(\alpha)$, frequency dependent SNR of the pressure P_{SNR} and particle velocity U_{SNR} for the absorber.

4.2 External source of white noise (ESWN)

The external source is positioned 10 m away from the receiver, with the angle θ = 0°, 30°, 60°, 90°. In this simulation scenario, the SNR of the pressure is fixed to 10 dB. Figure. 5 shows $E(\alpha)$, P_{SNR} and U_{SNR} with the receiver

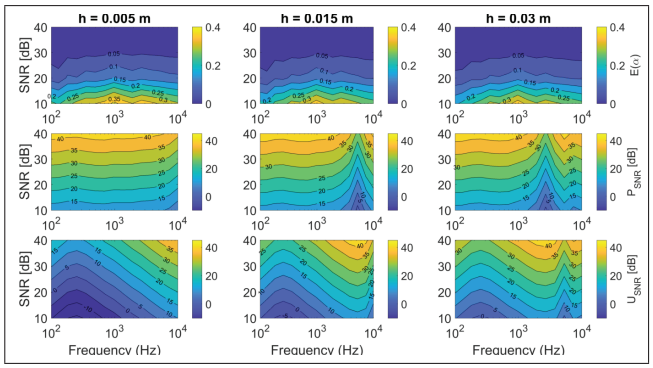

Figure 4. Absolute error of absorption coefficient $E(\alpha)$, frequency dependent SNR of the pressure P_{SNR} and particle velocity U_{SNR} for the reflector.

at 0.005 m. The black dashed line represents $E(\alpha)$ in the AWN case with the same SNR of the pressure, which is 10 dB.

First, it can be seen that $\theta = 0°$ shows peculiar behaviour compared to other angles. This can be explained that the Microflown particle velocity sensor has a figure-of-eight directivity pattern, which benefits the sensor to be insensitive to sound arriving from the sides [18]. This asset allows the reduction of background noise and enables the PU probe to be applied for in-situ measurements. Bearing this in mind, in the U_{SNR} plot, the SNR is much higher when the external source is at 0° than at other angles. No direct sound is received at the receiver, but only the reflected sound, which is strongly restricted due to the directivity. For the reflector, as the angle increases, U_{SNR} drops, and so does the accuracy of the absorption coefficient which is implied by the increase of $E(\alpha)$. This is not observed in the absorber though.

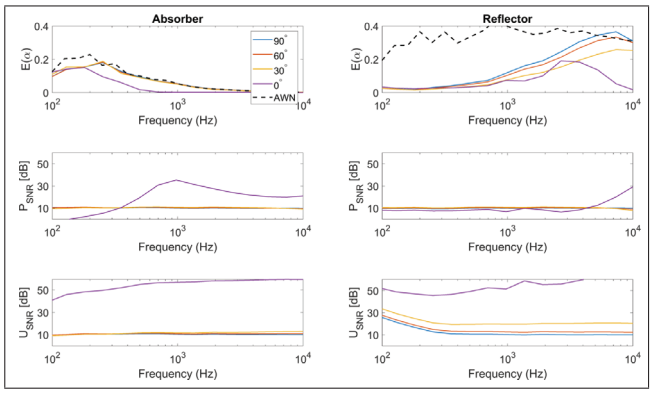

Figure 5. Absolute error of absorption coefficient $E(\alpha)$, frequency dependent SNR of the pressure P_{SNR} and particle velocity U_{SNR} for the absorber and reflector. The receiver height h = 0.005 m.

For the reflector, as the receiver height h increases, the overall $E(\alpha)$ increases, as in Figure. 6 and Figure. 7. At high frequencies above 1 kHz, $E(\alpha)$ shows no clear dependency on the angle θ. The frequency of the standing wave shifts to lower ranges as the receiver location rises. When the external source is at different angles, the frequency of the standing wave also shifts accordingly. The standing wave patterns of the external source overlaps with the pattern of the source, which results in irregular absorption error distribution. Similar as in Figure. 5, the receiver height h has no significant influence on the absorption error, except for a slight gain at low frequencies with increasing h. Opposite to the dependency on U_{SNR} in the AWN case, the ESWN case seems to depend more on P_{SNR}, especially at high frequencies and receiver height. Only when h = 0.005 m, $E(\alpha)$ is correlated with U_{SNR} and P_{SNR} when $\theta = 0°$.

Compared with the AWN case, the absorber shows quite similar $E(\alpha)$ distribution. While for the reflector, the error only deteriotes and get close to the error of the AWN case with a large receiver height.

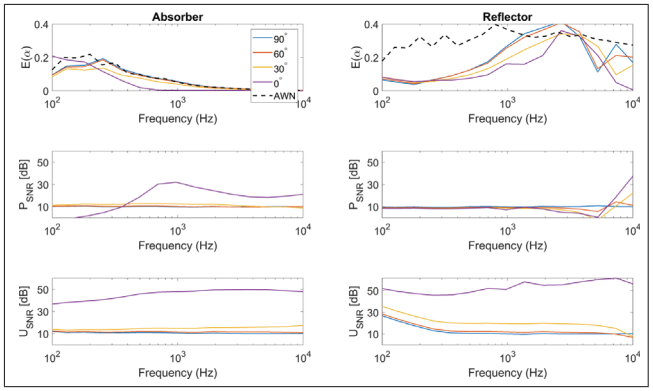

Figure 6. Absolute error of absorption coefficient $E(\alpha)$, frequency dependent SNR of the pressure P_{SNR} and particle velocity U_{SNR} for the absorber and reflector. The receiver height h = 0.015 m.

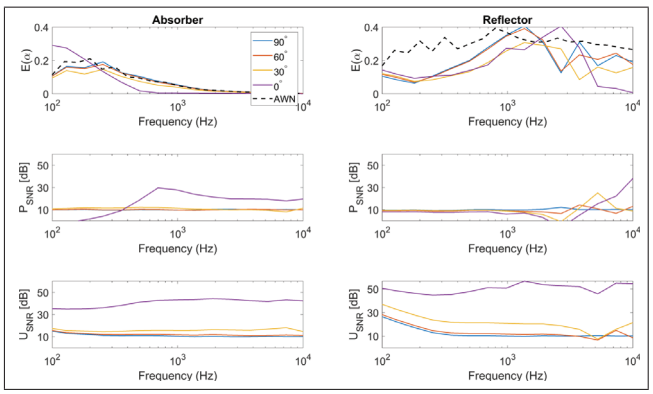

Figure 7. Absolute error of absorption coefficient $E(\alpha)$, frequency dependent SNR of the pressure P_{SNR} and particle velocity U_{SNR} for the absorber and reflector. The receiver height h = 0.03 m.

To summarize, the absorber is insensitive to the receiver height and the angle of a external source. Whereas for the reflector, a large receiver height impacts the accuracy of the calculated absorption coeffcient, more at high frequencies.

4.3 Considerations of quality indication in in-situ measurement environments

In the above two subsections, the scenarios of added white noise and external source with white noise are studied and compared. A real in-situ measurement environment mostly contains the two scenarios. Therefore, the results of the two scenarios need to be combined to provide quality indication. A quality indicator indicating acceptable background noise level (SNR) needs to be explored.

The absorber that represents absorbent materials, is insensitive to the receiver height h and the angle θ of an external source. Large errors of absorption coefficient $E(\alpha)$, including negative values, only exist at low frequencies, which can be indicated by the frequency dependent SNR of the particle velocity U_{SNR}. Since no large error is observed at high frequencies, the quality indicator in terms of SNR can be focused on the low-frequency U_{SNR}.

The quality indication of the reflector that represents reflective materials is more complicated. As h increases, $E(\alpha)$ decreases for the AWN case but increases for the ESWN case. Note that Figure. 4, or the dashed black curves in Figure. 5 to 7 exhibit that the decrease of $E(\alpha)$ of AWN is limited, whereas the $E(\alpha)$ increase in ESWN is more pronounced when the receiver location rises. Therefore, in an in-situ environment, it is recommended to keep the receiver as close as possible to the measured material surface to assure accurate absorption coefficient. For the AWN case, $E(\alpha)$ is more dependent on U_{SNR}; for the ESWN case, $E(\alpha)$ is more influenced by P_{SNR} at high frequenceis and large receiver heights. Only when the receiver is at 0.005 m, $E(\alpha)$ is correlated with U_{SNR}. In terms of SNR quality indicator, no frequency dependent $E(\alpha)$ is observed and U_{SNR} is not strongly correlated with $E(\alpha)$. Standing waves at high frequencies lead to large P_{SNR} deviations, and it causes large $E(\alpha)$. Therefore, high-frequency P_{SNR} can be an effective quality indicator to control $E(\alpha)$.

5. CONCLUSIONS

This work investigated the influence of background noise in in-situ absorption measurements based on PU method through simulations. The SNR of the background noise, two different types of background noise (SWN and ESWN), receiver height and two types of materials (absorber and reflector) were regarded as variables for the accuracy evaluation of the calculated absorption coefficient in the simulations. In general, a low receiver height contributes to high accuracy of deriving the absorption coefficient. For the absorber, it was found that the absorption coefficient is insensitive to the receiver height and the external source angle, and large deviations only exist at low frequencies. The deviation is highly correlated with the low-frequency SNR of particle velocity U_{SNR}, which can be used as SNR indicator for the absorber to control the error of the absorption coefficient. Whereas for the reflector, high-frequency P_{SNR} could be an effective SNR indicator to show a threshold of the quality of the signals for achieving certain absorption accuracy.

The presented conclusion is a good guideline to further explore quantitative SNR quality indicator. The future work includes investigating the relationship between the error of the absorption coefficient and the frequency dependent P_{SNR} and U_{SNR} for different materials, and in which frequency range to look into which SNR. Techniques of removing reflections not from the source would also be interesting to study. In addition, more quality indicators are required to fully understand uncertainties that might occur in the in-situ measurements, and to deliver confident measures of materials' acoustic characteristics.

6. REFERENCES

[1] E. Tijs, *Study and development of an in situ acoustic absorption measurement method*. PhD thesis, University of Twente, 2013.

[2] L. Savioja and U. P. Svensson, "Overview of geometrical room acoustic modeling techniques," *The Journal of the Acoustical Society of America*, vol. 138, no. 2, pp. 708–730, 2015.

[3] B. B. De La Hosseraye, H. Wang, F. Georgiou, M. Hornikx, and P. Robinson, "Derivation of time-domain surface impedance boundary conditions based on in-situ surface measurements and model fitting," in *23rd International Congress on Acoustics*, 2019.

[4] ISO, "10534-2," *coustics — Determination of sound absorption coefficient and impedance in impedance tubes — Part 2: Transfer-function method (ISO 10534-2)*, 1993.

[5] ISO, "354," *Acoustics — Measurement of sound absorption in a reverberation room (ISO 354)*, 2003.

[6] M. Müller-Trapet, P. Dietrich, M. Aretz, J. van Gemmeren, and M. Vorländer, "On the in situ impedance measurement with pu-probes—simulation of the measurement setup," *The Journal of the Acoustical Society of America*, vol. 134, no. 2, pp. 1082–1089, 2013.

[7] H.-E. de Bree, "An overview of microflown technologies," *Acta acustica united with Acustica*, vol. 89, no. 1, pp. 163–172, 2003.

[8] M. Aretz and M. Vorländer, "Combined wave and ray based room acoustic simulations of audio systems in car passenger compartments, part i: Boundary and source data," *Applied acoustics*, vol. 76, pp. 82–99, 2014.

[9] M. Li, W. van Keulen, E. Tijs, M. van de Ven, and A. Molenaar, "Sound absorption measurement of road surface with in situ technology," *Applied Acoustics*, vol. 88, pp. 12–21, 2015.

[10] E. Tijs, H. de Bree, and E. Brandão, "Large scale in situ acoustic reflection measurements in a theatre," in *Proc. of Nag/Daga*, pp. 549–552, 2009.

[11] B. Alvarez and F. Jacobsen, "An iterative method for determining the surface impedance of acoustic materials in situ," in *INTER-NOISE and NOISE-CON Congress and Conference Proceedings*, vol. 2008, pp. 4055–4065, Institute of Noise Control Engineering, 2008.

[12] E. Brandão, P. Mareze, A. Lenzi, and A. R. da Silva, "Impedance measurement of non-locally reactive samples and the influence of the assumption of local reaction," *The Journal of the Acoustical Society of America*, vol. 133, no. 5, pp. 2722–2731, 2013.

[13] E. Brandao, R. C. Flesch, A. Lenzi, and C. A. Flesch, "Estimation of pressure-particle velocity impedance measurement uncertainty using the monte carlo method," *The Journal of the Acoustical Society of America*, vol. 130, no. 1, pp. EL25–EL31, 2011.

[14] E. Brandão, A. Lenzi, and J. Cordioli, "Estimation and minimization of errors caused by sample size effect in the measurement of the normal absorption coefficient of a locally reactive surface," *Applied Acoustics*, vol. 73, no. 6-7, pp. 543–556, 2012.

[15] J. Hübelt, C. Kühnert, U. Figula, F. Wellner, and A. Blasl, "Acoustical method for non-destructive determination of porosity of asphalts," vol. 31, 10 2009.

[16] H. Kuttruff, *Acoustics: an introduction*. CRC Press, 2007.

[17] M. Delany and E. Bazley, "Acoustical properties of fibrous absorbent materials," *Applied acoustics*, vol. 3, no. 2, pp. 105–116, 1970.

[18] D. F. Comesana, *Scan-based sound visualisation methods using sound pressure and particle velocity*. PhD thesis, University of Southampton, 2014.